Publication Year	2016
Acceptance in OA@INAF	2020-07-07T08:45:51Z
Title	High-resolution Spectroscopy of a Young, Low-metallicity Optically Thin L = 0.02L* Star-forming Galaxy at z = 3.12
Authors	VANZELLA, Eros; De Barros, S.; CUPANI, Guido; Karman, W.; Gronke, M.; et al.
DOI	10.3847/2041-8205/821/2/L27
Handle	http://hdl.handle.net/20.500.12386/26353
Journal	THE ASTROPHYSICAL JOURNAL LETTERS
Number	821

The Astrophysical Journal Letters, 821:L27 (7pp), 2016 April 20
doi:10.3847/2041-8205/821/2/L27

HIGH-RESOLUTION SPECTROSCOPY OF A YOUNG, LOW-METALLICITY OPTICALLY THIN $L = 0.02L^*$ STAR-FORMING GALAXY AT $z = 3.12$*

E. Vanzella[1], S. De Barros[1], G. Cupani[2], W. Karman[3], M. Gronke[4], I. Balestra[2,5], D. Coe[6], M. Mignoli[1], M. Brusa[7], F. Calura[1], G.-B. Caminha[8], K. Caputi[3], M. Castellano[9], L. Christensen[10], A. Comastri[1], S. Cristiani[2], M. Dijkstra[4], A. Fontana[9], E. Giallongo[9], M. Giavalisco[11], R. Gilli[1], A. Grazian[9], C. Grillo[10], A. Koekemoer[6], M. Meneghetti[1], M. Nonino[2], L. Pentericci[9], P. Rosati[8], D. Schaerer[12], A. Verhamme[12], C. Vignali[7], and G. Zamorani[1]
[1] INAF–Osservatorio Astronomico di Bologna, via Ranzani 1, I-40127 Bologna, Italy; eros.vanzella@oabo.inaf.it
[2] INAF—Osservatorio Astronomico di Trieste, via G. B. Tiepolo 11, I-34131, Trieste, Italy
[3] Kapteyn Astronomical Institute, University of Groningen, Postbus 800, 9700 AV Groningen, The Netherlands
[4] Institute of Theoretical Astrophysics, University of Oslo, Postboks 1029 Blindern, NO-0315 Oslo, Norway
[5] University Observatory Munich, Scheinerstrasse 1, D-819 München, Germany
[6] STScI, 3700 San Martin Drive, Baltimore, MD 21218, USA
[7] Dipartimento di Fisica e Astronomia, Universitá degli Studi di Bologna, Viale Berti Pichat 6/2, I-40127 Bologna, Italy
[8] Dipartimento di Fisica e Scienze della Terra, Università di Ferrara, via Saragat 1, I-44122 Ferrara, Italy
[9] INAF–Osservatorio Astronomico di Roma, via Frascati 33, I-00040 Monteporzio, Italy
[10] Dark Cosmology Centre, Niels Bohr Institute, University of Copenhagen, Juliane Maries Vej 30, DK-2100 Copenhagen, Denmark
[11] Astronomy Department, University of Massachusetts, Amherst, MA 01003, USA
[12] Observatoire de Genève, Universit de Genève, 51 Ch. des Maillettes, 1290 Versoix, Switzerland
Received 2016 March 4; revised 2016 April 6; accepted 2016 April 7; published 2016 April 19

ABSTRACT

We present VLT/X-Shooter and MUSE spectroscopy of a faint F814W $= 28.60 \pm 0.33$ ($M_{\rm UV} = -17.0$), low-mass ($\lesssim 10^7 M_\odot$), and compact ($R_{\rm eff} = 62$ pc) freshly star-forming galaxy at $z = 3.1169$ magnified (16×) by the *Hubble Frontier Fields* galaxy cluster Abell S1063. Gravitational lensing allows for a significant jump toward low-luminosity regimes, in moderately high-resolution spectroscopy ($R = \lambda/d\lambda \sim 3000$–7400). We measured C IV λ1548, 1550, He II λ1640, O III]λ1661, 1666, C III]$\lambda\lambda$1907, 1909, Hβ, [O III]$\lambda\lambda$4959, 5007 emission lines with FWHM $\lesssim 50$ km s^{-1} and (de-lensed) fluxes spanning the interval 1.0×10^{-19}–2×10^{-18} erg s^{-1} cm^{-2} at signal-to-noise ratio (S/N) = 4–30. The double-peaked Lyα emission with Δv(red − blue) = 280(±7) km s^{-1} and de-lensed fluxes $2.4_{\rm (blue)}|8.5_{\rm (red)} \times 10^{-18}$ erg s^{-1} cm^{-2} (S/N = $38_{\rm (blue)}|110_{\rm (red)}$) indicate a low column density of neutral hydrogen gas consistent with a highly ionized interstellar medium as also inferred from the large [O III]λ5007/ [O II]λ3727 > 10 ratio. We detect C IV λ1548, 1550 resonant doublet in emission, each component with FWHM $\lesssim 45$ km s^{-1} and redshifted by +51(±10) km s^{-1} relative to the systemic redshift. We interpret this as nebular emission tracing an expanding optically thin interstellar medium. Both C IV λ1548, 1550 and He II λ1640 suggest the presence of hot and massive stars (with a possible faint active galactic nucleus). The ultraviolet slope is remarkably blue, $\beta = -2.95 \pm 0.20$ ($F_\lambda = \lambda^\beta$), consistent with a dust-free and young $\lesssim$20 Myr galaxy. Line ratios suggest an oxygen abundance 12 + log(O/H) < 7.8. We are witnessing an early episode of star formation in which a relatively low $N_{\rm H\,I}$ and negligible dust attenuation might favor a leakage of ionizing radiation. This galaxy currently represents a unique low-luminosity reference object for future studies of the reionization epoch with the *James Webb Space Telescope*.

Key words: cosmology: observations – galaxies: formation

1. INTRODUCTION

The epoch of reionization marks a major phase transition of the universe, during which the intergalactic space became transparent to UV photons. Determining when this occurred, the physical processes involved, and the sources of ionizing radiation represents one of the major goals in observational cosmology. The production of ionizing radiation is most probably driven by star formation and/or nuclear activity, but their relative contribution to the ionizing background is still matter of debate (e.g., Fontanot et al. 2014). Irrespective of the nature of ionizing radiation, the general consensus is that the faint sources are the main producers of the ionizing background at high redshift (Kimm & Cen 2014; Wise et al. 2014; Madau & Haardt 2015; but see Sharma et al. 2016). This implicitly assumes that a non-negligible fraction of ionizing photons is not trapped in faint sources and escapes. It is therefore important to push observations toward low-luminosity regimes ($L < 0.1L^\star$) to investigate the nature of ionizing radiation and the opacity at the Lyman continuum (LyC, <912 Å). Furthermore, high-ionization and narrow atomic transitions (like C IV λ1548, 1550, He II λ1640, C III]$\lambda\lambda$1907, 1909) recently identified at $z \sim 2$–3 and $z > 6$ raised intriguing questions about the presence of hot and massive stars and/or faint nuclear activity (e.g., Stark et al. 2014, 2015a) and/or possibly extreme stellar populations (Sobral et al. 2015). Also, the large [O III]λ5007 rest-frame equivalent width (>500–1000 Å) and [O III]λ5007/ [O II]λ3727 ratio (>5) recently observed in relatively bright ($L \simeq L^\star$) LyC-emitting galaxies is opening promising prospects for the characterization of reionizing sources at $z > 6$ (Jaskot & Oey 2013; Nakajima & Ouchi 2014; de Barros et al. 2016; Izotov et al. 2016; Vanzella et al. 2016). A subsequent step is to extend this study to fainter luminosity regimes. Here, we push observations to unprecedented luminosities limits ($L \simeq 0.02L^\star$, or F814W

* Based on observations collected at the European Southern Observatory for Astronomical research in the Southern Hemisphere under ESO programs P095.A-0840, P095.A-0653, P186.A-0798.

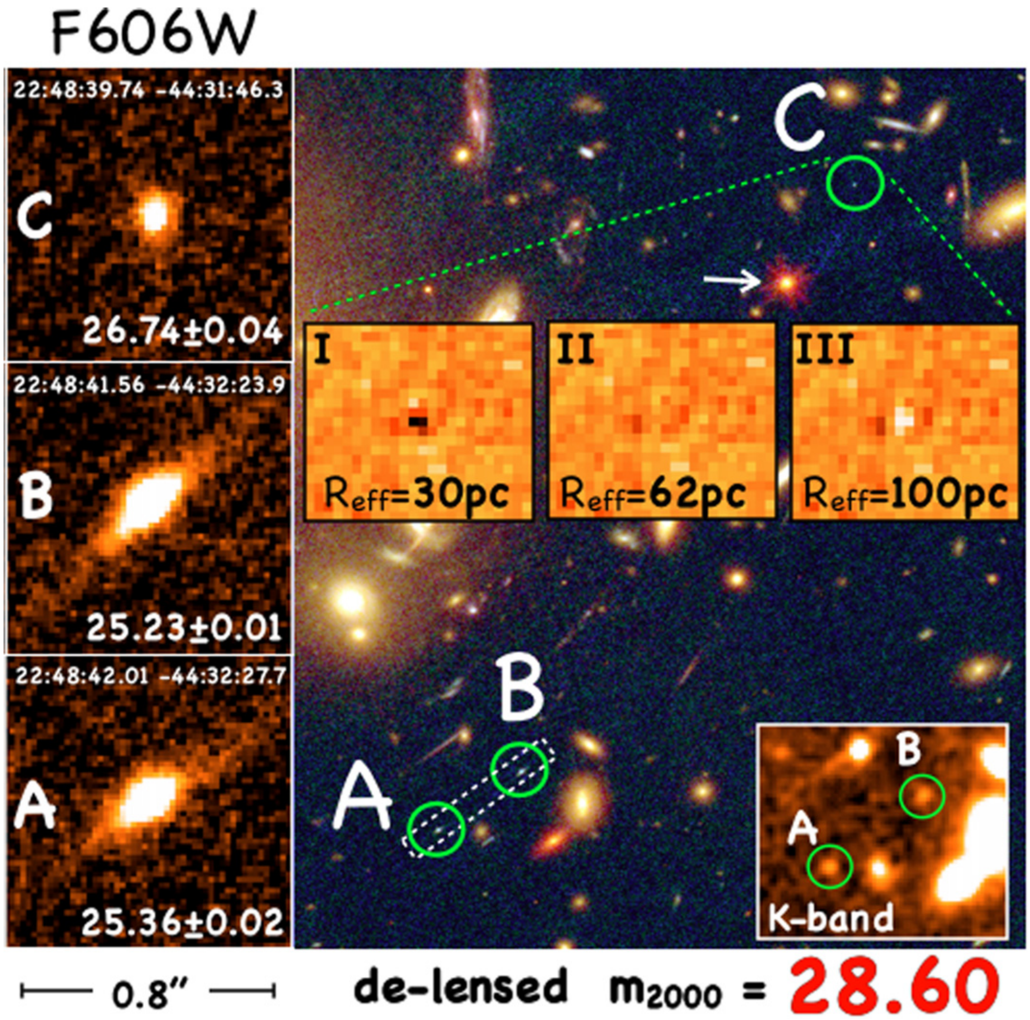

Figure 1. Left: the multiple images A, B, and C in the F606W band (S/N $\simeq$ 20–50), the observed magnitudes, and coordinates are shown. Right: the three multiple images are indicated with green circles over the color image (100″ × 80″), as well as the orientation and length of the X-Shooter slit (dotted line). The insets (I, II, III) show the residuals of the three Galfit models (0.″7 × 0.″9) with different de-lensed $R_{\rm eff}$ calculated on image C (F606W). The arrow indicates the star used as the PSF model. The bottom right panel shows images A and B in the VLT/K-band, boosted by nebular [O III]λλ4959, 5007 lines.

$\simeq$ 28.60) and ask the following questions. What is the nature of the ionizing radiation at very faint luminosity/mass domain? Are faint sources optically thin at the LyC as expected if they dominate reionization? Here, a detailed study of a faint galaxy is presented, taking advantage of multi-wavelength photometry available from the CLASH (Postman et al. 2012) and Hubble Frontier Fields (HFF) projects (Koekemoer et al. 2014; Lotz et al. 2014)[13] and from the low- and medium-resolution spectroscopy we obtained at VLT (VIMOS, MUSE, and X-Shooter).

2. TARGET SELECTION, MAGNIFICATION, AND X-SHOOTER OBSERVATIONS

The source ID11 has been selected among a sample of Lyα emitters identified with four-hour integration with MUSE behind the HFF galaxy cluster AS1063 (or RXJ2248; see Karman et al. 2015, K15 hereafter) and previously detected with VLT/VIMOS low-resolution spectroscopy ($R = 180$) by Balestra et al. (2013).

ID11 is a $z = 3.1169$ compact galaxy lensed into three images, A, B, and C, as shown in Figure 1. The A and B images have very similar F814W magnitudes, 25.65 ± 0.02 and 25.57 ± 0.02, respectively, while the third one (C) is the faintest with F814W = 27.06 ± 0.04 magnitude. Such a geometric configuration is well reproduced by the lensing modeling. The galaxy is close to a caustic on the source plane, and the corresponding critical line lies approximately between the two images A and B on the lens plane. Among the three images, the faintest one (C) has the least uncertain magnification factor, which is estimated to be $\mu_C = 4.1 \pm 0.2$ (Caminha et al. 2016). The magnification of the counter-images A and B have been calculated from the observed flux ratios between C and A, B, since the three images originate from the same source (Figure 1). The resulting magnifications are $\mu_A = 15.0$ and $\mu_B = 16.2$ with errors smaller than 10%, inferred from the photometry and the more accurate estimate of μ_C, and are consistent with those derived from lens modeling by Caminha et al. (2016). The de-lensed magnitude of the source in the F814W band (probing the continuum at $\simeq$2000 Å rest-frame) is 28.60 ± 0.33.

[13] http://www.stsci.edu/hst/campaigns/frontier-fields/

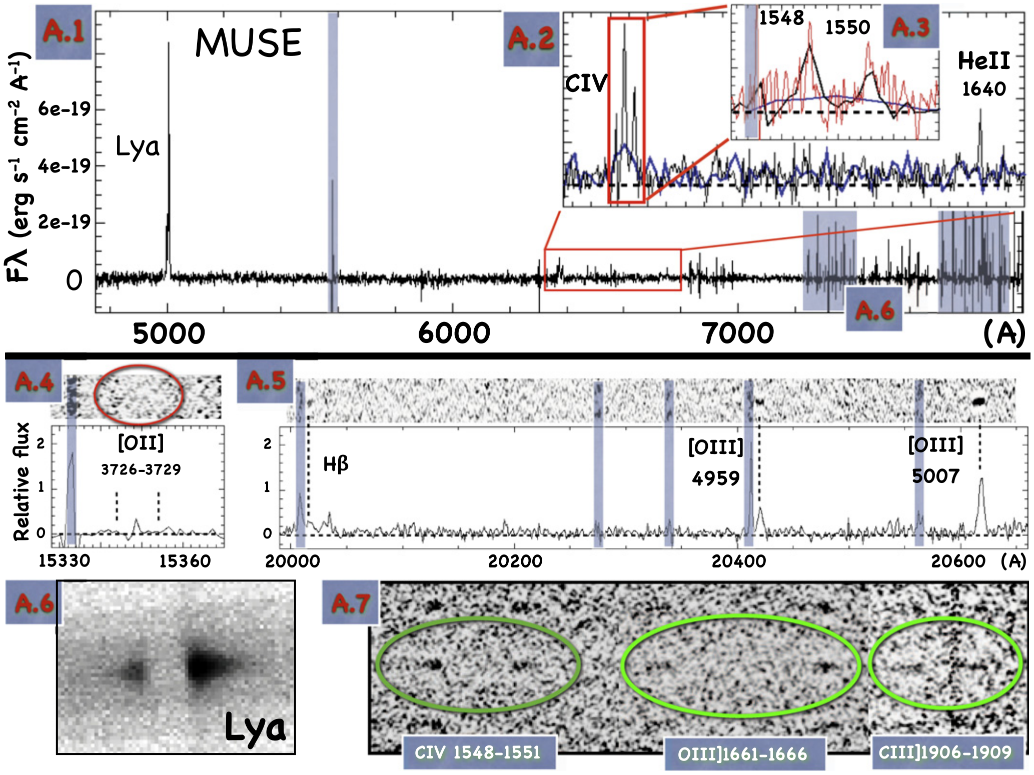

Figure 2. Top: the MUSE spectrum is shown (A.1) with the sky emission regions indicated (gray stripes). The zoomed MUSE region of C ivλ1548, 1550 and He ii λ1640 lines is shown (A.2). A low spectral resolution spectrum is shown ($R = 200$, blue line, A.2). A detail of the X-Shooter C ivλ1548, 1550 doublet is shown in A.3, red line, superimposed on MUSE and VIMOS spectra. Bottom: two-dimensional X-Shooter spectra zoomed around [O ii]λ3727, 3729 (A.4), Hβ + [O iii]$\lambda\lambda$4959, 5007 (A.5), Lyα (A.6), C ivλ1548, 1550, O iii]λ1661, 1666, and C iii]$\lambda\lambda$1907, 1909 (A.7) are shown. The Lyα line is the sum of the two images A and B computed directly on the raw science frames. The green ellipses indicate lines after summing the two sky-subtracted images A and B (4 hr) and shifting the spectra properly along the spatial direction. The emissions above and below the ellipses are the single exposures (2 hr).

The VLT/X-Shooter (Vernet et al. 2011) observations of source ID11 have been performed by inserting components A and B in the slit (Figure 1). Out of the four hours requested only two have been executed. However, combining the two counter-images A and B, the equivalent of four hours of integration have been achieved with a spectral resolution R of 5000, 7350, and 5100 in the three UVB ($\simeq$3000–5600 Å), VIS ($\simeq$5500–10000 Å), and NIR ($\simeq$10000–23700 Å) arms, respectively.

Particular care has been devoted to the data reduction of such a faint object. The data were first reduced using the latest release of the ESO X-Shooter pipeline (Modigliani et al. 2010). The ESO pipeline produces rectified sky-subtracted spectra of the echelle orders that are useful to determine the position of the two A and B images along the slit. With this information, a model of the sky emission on the science exposure has been calculated with the technique described in Kelson (2003).[14] Wavelength calibration was performed using arc lamp lines (for the UVB arm) or the sky emission lines (for the VIS and NIR arms); the resulting rms was typically 1/10 pixels. As a further check, the wavelength positions of the emission lines are fully consistent with what derived from MUSE. The combined 1D spectrum was optimally extracted from the wavelength- and flux-calibrated 2D spectra. A resolution-optimized velocity binning was adopted for the three arms (20, 11, and 19 km s^{-1} for the UVB, VIS, and NIR, respectively).

[14] It has been performed with a specific IDL pipeline developed by George Becker.

The reduced spectrum and the zoomed Lyα line are shown in Figures 2 and 3, respectively.

3. RESULTS FROM SPECTROSCOPY AND MULTI-BAND PHOTOMETRY

3.1. Spectral Properties

The double-peaked Lyα line was initially detected with MUSE (K15). The two components of the doublet are resolved in the X-Shooter spectrum, in which the asymmetric shape with a trough toward the systemic velocity is evident (see Figure 3).

As already discussed in K15, faint high-ionization emission lines have been detected (C iv λ1548, 1550, He ii λ1640, O iii]λ1661, 1666) but not resolved at the MUSE spectral resolution, placing a limit of FWHM < 100 km s^{-1} (instrumental corrected). As the Lyα line is the brightest feature in the MUSE data, we used it to create a mask to extract the spectra. Although this leads to a higher signal-to-noise ratio (S/N) and better flux measurement of Lyα, the high-ionization lines do not have enough S/N in the outer parts of this mask and are therefore detected with lower S/N. We therefore used the mask to extract the Lyα flux, but used a circular 1″ radius aperture to measure the high-ionization lines and verified that these fluxes are in agreement with the fluxes in the full Lyα-mask.

While MUSE reaches deeper flux limits with a resolution element >100 km s^{-1}, the X-Shooter spectral resolution allows us to investigate the width of the features down to few tens of kilometers per second and better resolve emission lines close to

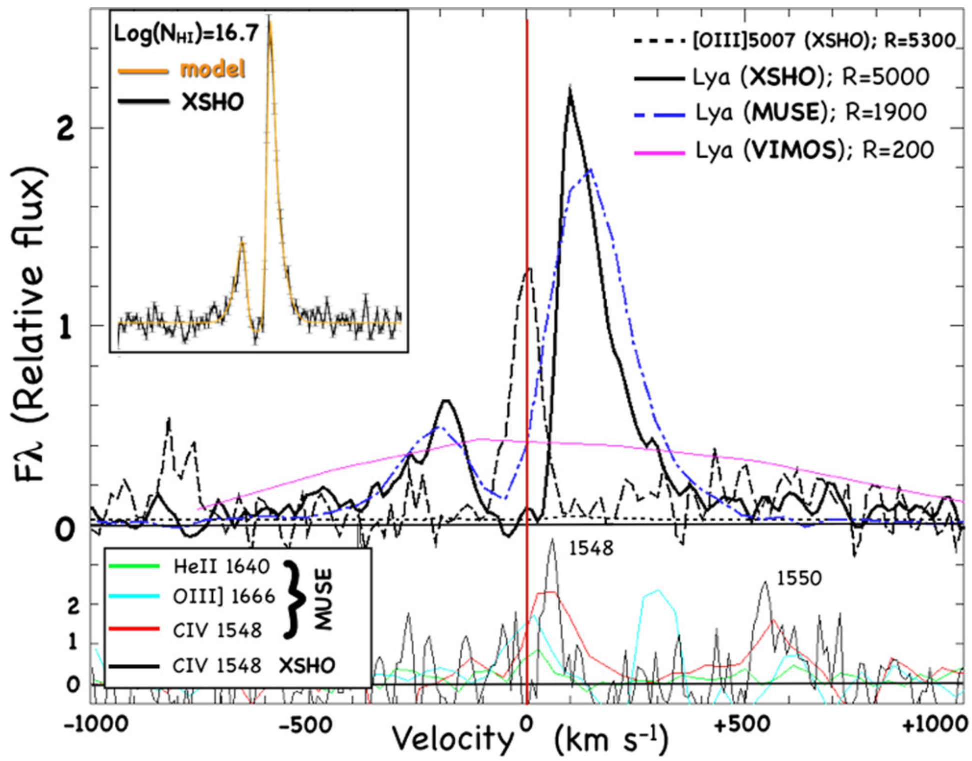

Figure 3. Comparison of the most relevant spectral features in the velocity space. Top panel: the Lyα line profile is shown for different instruments (VIMOS, MUSE, X-Shooter). The [O III]λ5007 emission line identified with X-Shooter is shown with a dashed line and marks the assumed systemic velocity (it has been multiplied by a factor of four for graphic purposes). Both components of the Lyα line are clearly resolved at the X-Shooter spectral resolution. The inset shows an example of Lyα modeling (orange line). Bottom panel: the high-ionization emission lines (as indicated in the legend) are also shown with respect to the systemic velocity. Among them, the only feature showing a significant velocity offset is the C IV λ1548, 1550 doublet, with $dv = +50$ km s^{-1}.

the sky emission. We anchor the flux measurements in the VIS arm to the MUSE ones (e.g., C IV λ1548, 1550 doublet), therefore accounting for slit losses and deriving X-Shooter fluxes for other lines missed in MUSE due to sky contamination. In particular, all the high-ionization lines identified in the X-Shooter spectrum show an FWHM of $\lesssim$50 km s^{-1} (see Table 1). It is worth noting that an accurate identification of such narrow lines in high-redshift star-forming galaxies is often compromised in low-resolution spectra (e.g., panel A.2 of Figure 2, blue line). The equivalent widths of the lines have been estimated from the line fluxes and the underlying continuum derived from SED fits (see below).

Furthermore, the near-infrared coverage of X-Shooter (up to 2.3 μm) allowed us to detect optical rest-frame emission lines like Hβ and [O III]$\lambda\lambda$4959, 5007 from which an accurate estimate of the systemic redshift is performed. In particular, from Hβ, [O III]$\lambda\lambda$4959, 5007 and ultraviolet O III]λ1661, 1666 and C III]λ1908 lines, we derived $z_{syst} = 3.1169 \pm 0.0002$. The high-ionization emission line redshifts are consistent with z_{syst}, except the C IV λ1548, 1550 components that show a clear velocity shift of $+51(\pm10)$ km s^{-1} (Figure 3). Moreover, the observed [O III]5007/[O II]3727 ratio (O32 index) is large ($>$10). We discuss below the possible interpretation of such features.

It is worth noting that at the given spectral resolution R = 5000–7000 and S/N of line fluxes, the X-Shooter spectrum presented here resembles what a 40 m class telescope can achieve in few hours integration time for an unlensed object of the same absolute magnitude and redshift (Disseau et al. 2014; Evans et al. 2015).

Table 1
Observed Spectral Lines

Line/Vacuumλ(Å)	Flux(S/N)[FWHM][EW]	Redshift
Lyα(blue)λ1215.69	3.15(38)[104][25]	3.1145
Lyα(red)λ1215.69	14.53(110)[104][116]	3.1184
C IVλ1548.20	0.52(18)[<45][7]	3.1177
C IVλ1550.78	0.29(10)[<45][4]	3.1175
He IIλ1640.42	0.21(6)[<100][3]	3.1169[a]
O III] λ1660.81	0.20(3)[<45][3]	(3.1167)[a]
O III] λ1666.15	0.31(5)[<45][5]	3.1169
[C III] λ1906.68	0.28(4)[<45][6]	3.1169
C III] λ1908.73	0.22(2)[<45][5]	(3.1170)
[O II]λ3727.09	<0.2	…
[O II]λ3729.88	<0.2	…
H$\beta\lambda$4862.69	0.31(4)[–][≃110]	(3.1166)
[O III] λ4960.30	0.90(12)[54][≃340]	3.1168
[O III] λ5008.24	2.35(33)[51][≃860]	3.1169

Note. Observed fluxes are reported in units of 10^{-17} ergs^{-1} cm^{-2} (de-lensed fluxes can be obtained by multiplying the values by 0.06). The S/N, FWHM (instrumental corrected, km s^{-1}), and rest-frame equivalent width (Å) are also indicated. The reported fluxes in the wavelength range 1215.68–1660.81 Å are estimated from MUSE. The FWHM, except He II1640, is estimated from the higher-resolution X-Shooter spectrum. Redshifts in parenthesis are uncertain due to low S/N.
[a] Indicates redshifts measured from the MUSE spectrum.

3.2. Modeling the Lyα Profile

The separation of the double-peaked Lyα line $\Delta_{peaks} = 280(\pm7)$ km s^{-1} is smaller than that commonly found at this redshift. Kulas et al. (2012) reported typical separations from 400 up to 1000 km s^{-1} for brighter L^* galaxies. It is instead slightly lower than the case reported by Christensen et al. (2012) in a lensed galaxy at $z = 1.83$, in which narrow C IV λ1548, 1550 emission was also detected.

The observed small separation suggests that $N_{\rm H\,I}$ is low. Specifically, we modeled the Lyα structure with the expanding shell model presented in Gronke et al. (2015) and described in W. Karman et al. (2016, in preparation). We refer the reader to those works for details. Under the model assumptions, a relatively narrow range of $N_{\rm H\,I}$ is allowed, $N_{\rm H\,I} \simeq 10^{16-18.5}$ cm^{-2} (an example is shown in the inset of Figure 3). This result is fully consistent with the analysis of Verhamme et al. (2015). In particular, it is worth noting that, given the estimated range for $N_{\rm H\,I}$, a leakage of ionizing radiation is also possible (i.e., $\tau_{\rm LyC} < 1$ if $N_{\rm H\,I} < 10^{17.2}$ cm^{-2}). An outflow velocity of $\simeq$55($\pm$10) km s^{-1} is also derived from the same modeling, fully consistent with the velocity offset inferred from the C IV λ1548, 1550 line doublet (see below). It is worth mentioning that fast outflows (>100 km s^{-1}) can mimic low $N_{\rm H\,I}$ when inferred from the Lyα profile (Schaerer et al. 2011; Verhamme et al. 2015). However, the low-velocity expansion derived from the C IV λ1548, 1550 doublets supports a low $N_{\rm H\,I}$ for this galaxy (<$10^{18.5}$ cm^{-2}).

*3.3. The C*IVλ1548, 1550 *Doublet and Optical Oxygen Lines*

Other evidence supporting a transparent medium is the presence of nebular C IVλ1548, 1550 emission. The C IVλ1548, 1550 doublet is a resonant transition and is very rarely observed with such narrow components in emission, possibly due to the low spectral resolution and limited depth of the current spectroscopic surveys. The C IVλ1548, 1550 transition is a combination of stellar P-Cygni emission and broad absorption (e.g., Kudritzki 2002), possible nebular emission, and interstellar absorption superposed (Shapley et al. 2003). In our case, the very thin lines ($\sigma_v \leqslant 20$ km s^{-1}) suggest that the interstellar medium is transparent, allowing the C IVλ1548, 1550 nebular emission to emerge. This is consistent with the low $N_{\rm H\,I}$ inferred from Lyα modeling mentioned above. Furthermore, the doublet is also redshifted by $\simeq$51 $\pm$ 10 km s^{-1} ($z = 3.1176$) compared to the systemic velocity ($z_{\rm syst} = 3.1169$). The measured velocity shift is consistent with the velocity expansion inferred from the Lyα modeling and can be ascribed to thin nebular emission from a moving medium.

Optical rest-frame oxygen emission lines also trace the status of the ISM. In particular, a large O32 ([O III]5007/[O II] 3727 > 10) index has been recently found in a LyC emitter at $z = 3.212$ (de Barros et al. 2016), for which escaping ionizing radiation has been confirmed with *Hubble Space Telescope* (*HST*) observations (Vanzella et al. 2016). The source described in this work shows a large O32 index (>10), plausibly linked to a low $N_{\rm H\,I}$, similarly to what is inferred from the Lyα and C IV λ1548, 1550 features discussed above. Such a large O32 index would suggest a density-bounded ISM, highly photoionized, in which the [O II]λ3727 emission is deficient (e.g., Jaskot & Oey 2013; Nakajima & Ouchi 2014).

3.4. A Newborn Low-metallicity Compact Galaxy

Multi-band imaging from the CLASH survey (Postman et al. 2012), recent deep *HST*/Advanced Camera for Surveys (ACS) observations part of the HFF program (F435W, F606W, and F814W), and additional archival *HST* data have been collected and combined to produce the photometric SED shown in Figure 4 (photometry has been extracted following Coe et al. 2015). We also retrieved and reduced the VLT/HAWKI Ks-band images from the ESO archive (P095.A-0533, PI: Brammer) and added it to the SED (see W. Karman et al. 2016, in preparation). The physical properties have been derived by performing SED fitting with Bruzual & Charlot (2003) models on both the A and B images, and accounting for nebular emission by fixing the emission line ratios to the observed ones (Schaerer & de Barros 2009, 2010). The fits have been carried out by including/excluding the bands affected by IGM and strong emission lines (Lyα and [O III]$\lambda\lambda$4959, 5007). The inferred physical quantities agree well in both cases and for the two counter-images (Figure 4). The K-band magnitudes dominated by the [O III]$\lambda\lambda$4959, 5007 lines and are well recovered even when the same band is excluded from the fit. Remarkably, an extremely blue ultraviolet slope is derived for the two images, from colors directly (e.g., Castellano et al. 2012) and from the best-fit SED, $\beta = -2.95 \pm 0.12$ and $\beta = -2.7 \pm 0.1$, respectively (see Figure 4). Such a blue shape is compatible with a dust-free and newborn galaxy with an emergent stellar component of $\lesssim$20Myr. The stellar mass turns out to be $M_\star \lesssim 10^7 M_\odot$. We derived the galaxy metallicity based on the direct T_e method from the O III]λ1666/ [O III]λ5007 ratio, which gives an electron temperature $T_e = 26500 \pm 2600$ K (Villar-Martín 2004). Following Izotov et al. (2006) and given O32 >10, we derive an oxygen abundance 12 + log(O/H) < 7.8.

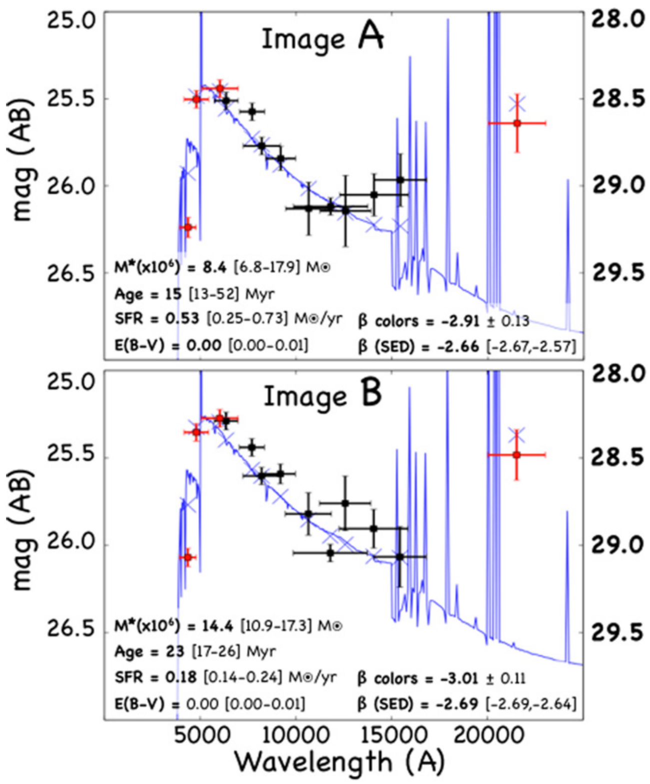

Figure 4. SED fits with Bruzual & Charlot templates are shown. The fits have been performed by both including and excluding the bands significantly contaminated by the IGM and emission lines (red points). The resulting physical quantities are reported with their 68% uncertainty. Observed and de-lensed magnitudes are reported in the *Y*-axis on the left and right side, respectively.

This places the galaxy in the low-mass and low-metallicity region of the mass–metallicity plane at $z \simeq 3$.

The ultraviolet emission arises from a spatially resolved region. From the F606W image of C (S/N > 20), which has better constrained magnification ($\mu_C = 4.1 \pm 0.2$), the (delensed) half-light radius is $R_{\rm eff} = 62(\pm 15)$pc. The $R_{\rm eff}$ and the uncertainty have been derived with Galfit (Peng et al. 2010) following the method described in Vanzella et al. (2015, 2016). Figure 1 shows three examples of observed-model residuals for three $R_{\rm eff}$ in the F606W band: 30, 62, and 100 pc, corresponding to 0.30 (unresolved), 0.55, and 1.00 pixels (1 pix = 0.″03). A similar solution is obtained from the F814W (C), $R_{\rm eff} \simeq 67$ pc. Such a small size, coupled with the aforementioned properties, is reminiscent of that observed in a $z \sim 3.212$ LyC emitter (Vanzella et al. 2016), though in the present case the source is more than three magnitudes fainter and four times smaller.

4. DISCUSSION AND CONCLUSIONS

4.1. The Nature of the Ionizing Radiation

The comparison of line ratios like C IV λ1550/He II λ1640, C IV λ1550/C III]λ1908, O III]λ1666/He II λ1640, C III]λ1908/He II λ1640 with models of Feltre et al. (2016) places the source among the star-forming galaxies, though still close to the active galactic nucleus (AGN) cloud, similarly to the blue galaxies of Stark et al. (2014). Such models are not conclusive for our object; however, they do not consider a possible leakage of ionizing radiation that could alter the expected ratios both for the UV and optical rest-frame lines, as, for example, happens for the O32 index (Nakajima & Ouchi 2014). While the high-ionization lines are compatible with an AGN, other properties suggest that the stellar emission is dominating: the source is spatially resolved in all the *HST*/ACS images, the very narrow widths of the involved emission lines (FWHM < 50 km s^{-1}) and the extremely blue slope are not typically observed in AGN-powered objects. Also, the redshifted C IV λ1548, 1550 doublet seems to contrast the ubiquitous blueshift observed in the AGN, though at brighter luminosities (e.g., Richards et al. 2011). Therefore, while all of our data can be interpreted with hot and massive stars ($T > 50{,}000$ K; Raiter et al. 2010; Gräfener & Vink 2015), only some of them appear to be consistent with the presence of a faint AGN.

4.2. A Young and Naked Galaxy: A Candidate Low-luminosity LyC Emitter

The observed spectroscopic and photometric properties in such an intrinsically faint (F814W(AB) = 28.60) galaxy can be measured only as a result of the factor of ≃16 magnification. The object is a compact ($R_{\rm eff} = 62$ pc), young (≲20 Myr), low-mass ($\lesssim 10^7 M_\odot$), and dust-free galaxy, with an ionizing source able to generate a density-bounded condition in the interstellar medium as inferred from the large O32 index. Such a transparent medium would therefore enable the young stellar component to dominate the emission and produce the steep ultraviolet slope. The redshifted C IV λ1548, 1550 nebular emission is also in line with an expanding optically thin medium. In addition, the very narrow double-peaked Lyα profile ($\Delta_v = 280$ km s^{-1}), the proximity of the red Lyα peak to the systemic redshift (≃100 km s^{-1}), and the low-velocity outflow suggest a low $N_{\rm H\,I}$ ($10^{16-18.5}$ cm^{-2}). Finally, as discussed by Raiter et al. (2010), the case of an escaping ionizing radiation would generate a depression of the nebular continuum that further favors a steepening of the ultraviolet slope, enhancing the equivalent width of the faint lines like He IIλ1640 or C III]λ1908, otherwise washed out by the continuum.

The thinness of the medium is noteworthy in this object and opens up the possibility that it is a LyC emitter. Irrespective of possible LyC leakage, the analysis addresses for the first time a still unexplored luminosity and mass domain and provides a unique reference lower-redshift analog to the higher-redshift blue sources ($z > 6$) at similar luminosities, believed to be the main actors during reionization (Atek et al. 2015; Bouwens et al. 2015; Castellano et al. 2016). It will be crucial to extend the analysis to a statistically significant sample and fainter luminosity limits.

Even though these extremely blue galaxies could be rare at $z \sim 3$, it might not be the case at $z > 6$, as the β-luminosity relations of Bouwens et al. (2014) seems to indicate. In particular, at $z \sim 7$, an average $\beta \simeq -2.8$ is expected at the luminosity probed here ($M_{\rm UV} = -17.0$; see also Finkelstein et al. 2012). In particular, the C IV λ1548, 1550 doublet discovered at $z = 7.04$ by Stark et al. (2015b) would be interesting to compare with the source discussed here.

Finally, we note that the initial phases of star formation as observed here offer the opportunity to test models of galaxy formation and photoionization effects in low-mass objects for the first time.

We thanks the anonymous referee for a helpful report. We acknowledge G. Becker for valuable support on the X-Shooter data reduction. We thanks R. Amorin for discussions about the metallicity of the object and M. Bellazzini and E. Carretta for useful discussions. Part of this work has been funded through the PRIN INAF 2012. M.M. acknowledges support from PRIN-INAF2014 1.05.01.94.02, ASI/INAF/I/023/12/0, and MAECI (US16GR08).

REFERENCES

Atek, H., Richard, J., Kneib, J.-P., et al. 2015, ApJ, 800, 18
Balestra, I., Vanzella, E., Rosati, P., et al. 2013, A&A, 559, L9
Bouwens, R. J., Illingworth, G. D., Oesch, P. A., et al. 2014, ApJ, 793, 115
Bouwens, R. J., Illingworth, G. D., Oesch, P. A., et al. 2015, ApJ, 803, 34
Bruzual, G., & Charlot, S. 2003, MNRAS, 344, 1000
Caminha, G. B., Grillo, C., Rosati, P., et al. 2016, A&A, 587, A80
Castellano, M., Dayal, P., Pentericci, L., et al. 2016, ApJL, 818, L3
Castellano, M., Fontana, A., Grazian, A., et al. 2012, A&A, 540, A39
Christensen, L., Laursen, P., Richard, J., et al. 2012, MNRAS, 427, 1973
Coe, D., Bradley, L., & Zitrin, A. 2015, ApJ, 800, 84
de Barros, S., Vanzella, E., Amorín, R., et al. 2016, A&A, 585, A51
Disseau, K., Puech, M., Flores, H., et al. 2014, Proc. SPIE, 9147, 914791
Evans, C., Puech, M., Afonso, J., et al. 2015, arXiv:1501.04726
Feltre, A., Charlot, S., & Gutkin, J. 2016, MNRAS, 456, 3354
Finkelstein, S. L., Papovich, C., Salmon, B., et al. 2012, ApJ, 756, 164
Fontanot, F., Cristiani, S., Pfrommer, C., Cupani, G., & Vanzella, E. 2014, MNRAS, 438, 2097
Gräfener, G., & Vink, J. S. 2015, A&A, 578, L2
Gronke, M., Bull, P., & Dijkstra, M. 2015, ApJ, 812, 123
Izotov, Y. I., Orlitová, I., Schaerer, D., et al. 2016, Natur, 529, 178
Izotov, Y. I., Stasińska, G., Meynet, G., Guseva, N. G., & Thuan, T. X. 2006, A&A, 448, 955
Jaskot, A. E., & Oey, M. S. 2013, ApJ, 766, 91
Karman, W., Caputi, K. I., Grillo, C., et al. 2015, A&A, 574, A11
Kelson, D. D. 2003, PASP, 115, 688
Kimm, T., & Cen, R. 2014, ApJ, 788, 121
Koekemoer, A. M., Avila, R. J., Hammer, D., et al. 2014, in BAAS, 223, 254.02
Kudritzki, R. P. 2002, ApJ, 577, 389

Kulas, K. R., Shapley, A. E., Kollmeier, J. A., et al. 2012, ApJ, 745, 33
Lotz, J., Mountain, M., Grogin, N. A., et al. 2014, in BAAS, 223, 254.01
Madau, P., & Haardt, F. 2015, ApJL, 813, L8
Modigliani, A., Goldoni, P., Royer, F., et al. 2010, Proc. SPIE, 7737, 773728
Nakajima, K., & Ouchi, M. 2014, MNRAS, 442, 900
Peng, C. Y., Ho, L. C., Impey, C. D., & Rix, H.-W. 2010, AJ, 139, 2097
Postman, M., Coe, D., Benítez, N., et al. 2012, ApJS, 199, 25
Raiter, A., Schaerer, D., & Fosbury, R. A. E. 2010, A&A, 523, A64
Richards, G. T., Kruczek, N. E., Gallagher, S. C., et al. 2011, AJ, 141, 167
Schaerer, D., & de Barros, S. 2009, A&A, 502, 423
Schaerer, D., & de Barros, S. 2010, A&A, 515, A73
Schaerer, D., Hayes, M., Verhamme, A., & Teyssier, R. 2011, A&A, 531, A12
Shapley, A. E., Steidel, C. C., Pettini, M., & Adelberger, K. L. 2003, ApJ, 588, 65
Sharma, M., Theuns, T., Frenk, C., et al. 2016, MNRAS, 458, L94
Sobral, D., Matthee, J., Darvish, B., et al. 2015, ApJ, 808, 139
Stark, D. P., Richard, J., Charlot, S., et al. 2015a, MNRAS, 450, 1846
Stark, D. P., Richard, J., Siana, B., et al. 2014, MNRAS, 445, 3200
Stark, D. P., Walth, G., Charlot, S., et al. 2015b, MNRAS, 454, 1393
Vanzella, E., de Barros, S., Castellano, M., et al. 2015, A&A, 576, A116
Vanzella, E., de Barros, S., Vasei, K., et al. 2016, arXiv:1602.00688
Verhamme, A., Orlitová, I., Schaerer, D., & Hayes, M. 2015, A&A, 578, A7
Vernet, J., Dekker, H., D'Odorico, S., et al. 2011, A&A, 536, A105
Villar-Martín, M., Cerviño, M., & González Delgado, R. M. 2004, MNRAS, 355, 1132
Wise, J. H., Demchenko, V. G., Halicek, M. T., et al. 2014, MNRAS, 442, 2560